J|A|C|S
ARTICLES
Published on Web 04/07/2006

Fluorocarbon-Modified Organic Semiconductors: Molecular Architecture, Electronic, and Crystal Structure Tuning of Arene- versus Fluoroarene-Thiophene Oligomer Thin-Film Properties

Myung-Han Yoon, Antonio Facchetti,* Charlotte E. Stern, and Tobin J. Marks*

Contribution from the Department of Chemistry and the Materials Research Center, Northwestern University, 2145 Sheridan Road, Evanston, Illinois, 60208

Received January 2, 2006; E-mail: t-marks@northwestern.edu; a-facchetti@northwestern.edu

Abstract: We present here the systematic synthesis and comparative physicochemical characterization of a series of regiochemically varied and core size extension-modulated arene(perfluoroarene)−thiophene oligomers. The molecules investigated are: 5,5″-diphenyl-2,2′:5′,2″:5″,2‴-quaterthiophene (**1**), 5,5′-bis-{1-[4-(thien-2-yl)phenyl]}-2,2′-dithiophene (**2**), 4,4′-bis[5-(2,2′-dithiophenyl)]-biphenyl (**3**), 5,5″-diperfluorophenyl-2,2′:5′,2″:5″,2‴-quaterthiophene (**4**), 5,5′-bis{1-[4-(thien-2-yl)perfluorophenyl]}-2,2′-dithiophene (**5**), 4,4′-bis[5-(2,2′-dithiophenyl)]-perfluorobiphenyl (**6**), 5,5″-diperfluorophenyl-2,2′:5′,2″-tertthiophene (**7**), 5,5′-diperfluorophenyl-2,2′-dihiophene (**8**), and 5,5-diperfluorophenylthiophene (**9**). Trends in optical absorption and emission parameters, molecular structures as defined by single-crystal X-ray diffraction, as well as electrochemical redox processes are described. The morphologies and microstructures of the vapor-deposited films grown over a range of growth temperatures have also been characterized. Field-effect transistor (FET) measurements demonstrate that all of these materials are FET-active and, depending on the molecular architecture, exhibit comparably good p- or n-type mobility when optimum film microstructural order is achieved. A very large n-channel mobility of $\sim$0.5 cm^2/Vs with I_{on}/I_{off} ratios $> 10^8$ is achieved for films of **4**.

Introduction

During the past two decades, molecular and polymeric semiconducting materials based on conjugated (hetero)aromatic rings have been extensively investigated, with development efforts focusing on applications in a variety of electronic and optical devices.[1] Among these materials, phenylene−thiophene oligomers, developed independently by Hotta and Samulski,[2] have attracted much attention due to their potential as active components in organic light-emitting diodes (OLEDs), organic diode lasers, and p-type semiconductors in organic thin-film transistors (OTFTs).[3] In striking contrast to simple oligo/poly phenylenes and thiophenes, molecular mixing of the two aromatic ring types produces structural motifs characterized by a diversity of molecular shapes and physical properties, which in turn profoundly alters the physical properties.[3,4] Remarkable examples include enhanced light emission and low-threshold amplified spontaneous emission (ASE) from liquid crystalline polymer blends.[5] The results of Katz et al.[6] on OTFT-defined charge transport indicate that thin films of such co-oligomers can exhibit large hole (p-type semiconductor) or electron (n-type semiconductor) mobilities (μ), very large current modula-

(1) (a) Barbarella, G.; Melucci, M.; Sotgiu, G. *Adv. Mater.* **2005**, *17*, 1581. (b) *Printed Organic and Molecular Electronics*; Gamota, D. R., Brazis, P., Kalyanasundaram, X., Zhang, J., Eds.; Kluwer Academic Publishers: New York, 2004. (c) *Handbook of Oligo- and Polythiophenes*; Fichou, D., Ed.; Wiley-VCH: Weinheim, Germany, 1999. (d) *Handbook of Conductive Polymers*; Skotheim, T. A., Elsenbaumer R. L., Reynolds, J. R., Eds.; Marcel Dekker: New York, 1998; pp 325−326. (e) Hotta, S. In *Handbook of Organic Conductive Molecules and Polymers*; Nalwa, H. S., Ed.; John Wiley & Sons: Chichester, U.K., 1997; Vol. 2, Chapter 8. (e) *Polythiophenes − Electrically Conductive Polymers*; Schopf, G., Kossmehl, G., Eds.: Springer, Berlin, 1997.

(2) (a) Hotta, S.; Lee, S. A. *Synth. Met.* **1999**, *101*, 551. (b) Dingemans, T. J.; Bacher, C. J.; Thelakkat, M.; Pederson, L. G.; Samulski E. T.; Schimidt, H.-W. *Synth. Met.* **1999**, *105*, 171.

(3) (a) Mohapatra, S.; Holmes, B. T.; Newman, C. R.; Prendergast, C. F.; Frisbie, C. D.; Ward, M. D. *Adv. Funct. Mater.* **2004**, *14*, 605. (b) Yanagi, H.; Araki, Y.; Ohara, T.; Hotta, S.; Ichikawa M.; Taniguchi, Y. *Adv. Funct. Mater.* **2003**, *13*, 767. (c) Casado, J.; Ruiz Delgado, M. C.; Shirota, Y.; Hernandez, V.; Lopez Navarrete, J. T. *J. Phys. Chem. B* **2003**, *107*, 2637. (d) Ichikawa, M.; Yanagi, H.; Shimizu, Y.; Hotta, S.; Suganuma, N.; Koyama T.; Taniguchi, Y. *Adv. Mater.* **2002**, *14*, 1272. (e) Apperloo, J. J.; Groenendaal, L. B.; Verheyen, H.; Jayakannan, M.; Janssen, R. A. J.; Dkhissi, A.; Beljonne, D.; Lazzaroni, R.; Bredas, J.-L. *Chemistry* **2002**, *8*, 2384. (f) Moreno Castro, C.; Ruiz Delgado, M. C.; Hernandez, V.; Hotta, S.; Casado, J.; Lopez Navarrete, J. T. *J. Phys. Chem. B* **2002**, *116*, 10419. (g) Lee, S. A.; Yoshida, Y.; Fukuyama M.; Hotta, S. *Synth. Met.* **1999**, *106*, 39. (h) Videlot-Ackermann, C., Ackermann, J.; Ackermann, J.; Brisset, H.; Kawamura, K.; Yoshimoto, N.; Raynal, P.; El Kassmi, A.; Fages, F. *J. Am Chem. Soc.* **2005**, *127*, 16346.

(4) (a) Hotta, S.; Katagiri, T. *J. Heterocycl. Chem.* **2003**, *40*, 845. (b) Hotta, S.; Kimura, H.; Lee, S. A.; Tamaki, T. *J. Heterocycl. Chem.* **2000**, *37*, 281. (c) Hotta, S.; Lee, S. A.; Tamaki, T. *J. Heterocycl. Chem.* **2000**, *37*, 25.

(5) (a) Yanagi, H.; Yoshiki, A.; Hotta, S.; Kobayashi, S *J. Appl. Phys.* **2004**, *96*, 4240. (b) Ichikawa, M.; Hibino, R.; Inoue, M.; Haritani, T.; Hotta, S.; Koyama, T.; Taniguchi, Y. *Adv. Mater.* **2003**, *15*, 213. (c) Nagawa, M.; Hibino, R.; Hotta, S.; Yanagi, H.; Ichikawa, M.; Koyama, T.; Taniguchi, Y. *Appl. Phys. Lett.* **2002**, *80*, 544. (d) Kim, Y. C.; Lee, T.-W.; Park, O.; Kim, C. Y.; Cho, H. N. *Adv. Mater.* **2001**, *13*, 646.

(6) . (a) Facchetti, A.; Letizia, J.; Yoon, M.-H.; Mushrush, M.; Katz, H. E.; Marks, T. J. *Chem. Mater.* **2004**, *16*, 4715. (b) Katz, H. E.; Siegrist, T.; Lefenfeld, M.; Gopalan, P.; Mushrush, M.; Ocko, B.; Gang, O.; Jisrawl, N. *J. Phys. Chem. B* **2004**, *108*, 8567. (c) Mushrush, M.; Facchetti, A.; Lefenfeld, M.; Katz, H. E.; Marks, T. J. *J. Am. Chem. Soc.* **2003**, *125*, 9414. (d) Hong, X. M.; Katz, H. E.; Lovinger, A. J.; Wang, B.-C.; Raghavachari, K. *Chem. Mater.* **2001**, *13*, 4686.

10.1021/ja060016a CCC: $33.50

Chart 1

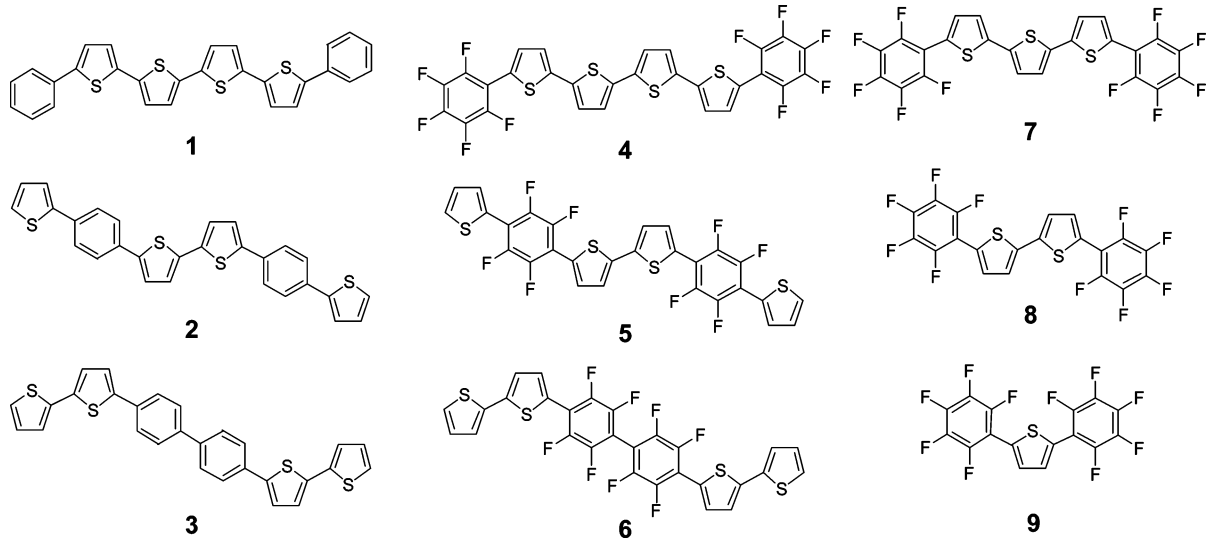

tion ratios (I_{on}/I_{off}), and unique OTFT nonvolatile memory characteristics compared to the parent oligothiophenes having the same number of constituent units.

In the quest for high-performance n-type OTFT-applicable semiconductors, to combine with the much broader p-type families[7] and to thereby achieve complementary circuits, a number of research groups[8,9] have made important contributions. We recently communicated in part[10] that perfluoroarene−thiophenes 5,5″-diperfluorophenyl-2,2′:5′,2″:5″,2‴-quaterthiophene (**4**), 5,5′-bis{1-[4-(thien-2-yl)perfluorophenyl]}-2,2′-dithiophene (**5**), and 4,4′-bis[5-(2,2′-dithiophenyl)]-perfluorobiphenyl (**6**) (Chart 1) exhibit unique molecular packing and charge transport characteristics. In this contribution we present a detailed investigation aimed at better understanding the properties of this oligothiophene class by comparing it to the corresponding fluorine-free analogues 5,5″-diphenyl-2,2′:5′,2″:5″,2‴-quaterthiophene (**1**), 5,5′-bis{1-[4-(thien-2-yl)phenyl]}-2,2′-dithiophene (**2**), and 4,4′-bis[5-(2,2′-dithiophenyl)]-biphenyl (**3**) and to oligomers with progressively contracted cores 5,5″-diperfluorophenyl-2,2′:5′,2″-tertthiophene (**7**), 5,5′-diperfluorophenyl-2,2′-dihiophene (**8**), and 5,5-diperfluorophenylthiophene (**9**). To this end, we report here the general synthesis of novel organic semiconductor classes **1**−**3** and **7**−**9**, on the basis of arene(fluoroarene)−thiophene building blocks, and the characterization of physical properties with respect to regiochemical modifications and oligothiophene core contraction using thermal analysis, optical spectroscopy, and cyclic voltametry. Single-crystal XRD structural data for the majority of these compounds are also presented and analyzed, and vapor-deposited film microstructures and morphologies are defined by XRD and SEM. Finally, OTFTs are fabricated and their device response discussed, focusing on the interplay between molecular electronic energy levels, crystal structure, and film microstructural characteristics. It will be seen that n-channel mobilities as high as ∼0.5 cm^2/Vs with $I_{on}/I_{off} > 10^8$ are achieved—unprecedented for an unsubstituted organic n-type semiconductor.

(7) (a) Meng, H.; Bendikov, M.; Mitchell, G.; Holgeson, R.; Wudl, F.; Bao, Z.; Siegrist, T.; Kloc, C.; Chen, C.-H. *Adv. Mater.* **2003**, *15*, 1090. (b) Santato, C.; Manunza, I.; Bonfiglio, A.; Cicoira, F.; Cosseddu, P.; Zamboni, R.; Muccini, M. *Appl. Phys. Lett.* **2005**, *86*, 141106/1. (c) Crouch, D. J.; Skabara, P. J.; Heeney, M.; McCulloch, I.; Coles, S. J.; Hursthouse, M. B. *Chem. Commun.* **2005**, 1465. (d) Li, D.; Borkent, E.-J.; Nortrup, R.; Moon, H.; Katz, H.; Bao, Z. *Appl. Phys. Lett.* **2005**, *86*, 042105/1. (e) Rang, Z.; Nathan, M. I.; Ruden, P. P.; Podzorov, V.; Gershenson, M. E.; Newman, C. R.; Frisbie, C. D. *Appl. Phys. Lett.* **2005**, *86*, 123501/1. (f) Tulevski, G. S.; Miao, Q.; Fukuto, M.; Abram, R.; Ocko, B.; Pindak, R.; Steigerwald, M. L.; Kagan, C. R.; Nuckolls, C *J. Am. Chem. Soc.* **2004**, *126*, 15048. (g) Sundar, V. C.; Zaumseil, J.; Podzorov, V.; Menard, E.; Willett, R. L.; Someya, T.; Gershenson, M. E.; Rogers, J. A. *Science* **2004**, *303*, 1644. (h) Gorjanc, T. C.; Levesque, I.; D′Iorio, M. *Appl. Phys. Lett.* **2004**, *84*, 930. (i) Katz, H. E.; Kloc, C.; Sundar, V.; Zaumseil, J.; Briseno, A. L.; Bao, Z. *J. Mater. Res.* **2004**, *19*, 1995. (j) Mohapatra, S.; Holmes, B. T.; Newman, C. R.; Prendergast, C. F.; Frisbie, C. D.; Ward, M. D. *Adv. Funct. Mater.* **2004**, *14*, 605. (k) Morin, J.-F.; Drolet, N.; Tao, Y.; Leclerc, M. *Chem. Mater.* **2004**, *16*, 4619. (l) Murphy, A. R.; Frechet, J. M. J.; Chang, P.; Lee, J.; Subramanian, V. *J. Am. Chem. Soc.* **2004**, *126*, 1596. (m) Sheraw, C. D.; Jackson, T. N.; Eaton, D. L.; Anthony, J. E. *Adv. Mater.* **2003**, *15*, 2009. (n) Meng, H.; Zheng, J.; Lovinger, A. J.; Wang, B.-C.; Van Patten, P. G.; Bao, Z. *Chem. Mater.* **2003**, *15*, 1778. (o) Afzali, A.; Dimitrakopoulos, C. D.; Graham, T. O. *Adv. Mater.* **2003**, *15*, 2066. (p) Locklin, J.; Li, D.; Mannsfeld, S. C. B.; Borkent, E.-J.; Meng, H.; Advincula, R.; Bao, Z. *Chem. Mater.* **2005**, *17*, 3366. (q) Halik, M.; Klauk, H.; Zschieschang, U.; Scmid, G.; Ponomarenko, S.; Kiechmayer, S.; Weber, W. *Adv. Mater.* **2003**, *15*, 917.

(8) (a) Yoon, M.-H.; DiBenedetto, S.; Facchetti, A.; Marks, T. J. *J. Am. Chem. Soc.* **2005**, *127*, 1348. (b) Facchetti, A.; Mushrush, M.; Yoon, M.-H.; Hutchison, G. R.; Ratner, M. A.; Marks, T. J. *J. Am. Chem. Soc.* **2004**, *126*, 13859. (c) Facchetti, A.; Yoon, M.-H.; Stern, C. L.; Hutchison, G. R.; Ratner, M *J. Am. Chem. Soc.* **2004**, *126*, 13480. (d) Jones, B. A.; Ahrens, M. J.; Yoon, M.-H.; Facchetti, A.; Marks, T. J.; Wasielewski, M. R. *Angew. Chem., Int. Ed.* **2004**, *43*, 6363. (e) Facchetti, A.; Mushrush, M.; Katz, H. E.; Marks, T. J. *Adv. Mater.* **2003**, *15*, 33. (f) Marks, T. J.; Facchetti, A. *WO Patent 0 310 778*, **2003**. (g) Facchetti, A.; Marks, T. J. *Polym. Prepr.* **2002**, *43(1)*, 734. (h) Marks, T. J.; Facchetti, A.; Sirringhaus, H.; Friend, R. H. *WO Patent 0 209 201*, **2002**. (i) Facchetti, A.; Deng, Y.; Wang, A.; Koide, Y.; Sirringhaus, H.; Marks, T. J.; Friend, R. H. *Angew. Chem., Int. Ed.* **2000**, *39*, 4547.

(9) (a) Chua, L.-L.; Zaumseil, J.; Chang, J.-F.; Ou, E. C.-W.; Ho, P. K.-H.; Sirringhaus, H.; Friend, R. H. *Nature* **2005**, *434*, 194. (b) Ando, S.; Nishida, J.; Tada, H.; Inoue, Y.; Tokito, S.; Yamashita, Y *J. Am. Chem. Soc.* **2005**, *127*, 5336. (c) Newman, C. R.; Frisbie, C. D.; da Silva Filho, D. A.; Bredas, J.-L.; Ewbank, P. C.; Mann, K. R. *Chem. Mater.* **2004**, *16*, 4436. (d) Mitzi, D. B.; Kosbar, L. L.; Murray, C. E.; Copel, M.; Afzali, A *Nature* **2004**, *428*, 299. (e) Sakamoto, Y.; Suzuki, T.; Kobayashi, M.; Gao, Y.; Fukai, Y.; Inoue, Y.; Sato, F.; Tokito, S. *J. Am. Chem. Soc.* **2004**, *126*, 8138. (f) Kunugi, Y.; Takimiya, K.; Toyoshima, Y.; Yamashita, K.; Aso, Y.; Otsubo, T. *J. Mater. Chem.* **2004**, *14*, 1367. (g) Chesterfield, R. J.; McKeen, J. C.; Newman, C. R.; Frisbie, C. D.; Ewbank, P. C.; Mann, K. R.; Miller, L. L *J. Appl. Phys.* **2004**, *95*, 6396. (h) Waldauf, C.; Schilinsky, P.; Perisutti, M.; Hauch, J.; Brabec, C. J. *Adv. Mater.* **2003**, *15*, 2084. (i) Facchetti, A., Yoon, M.-H.; Stern, C. L.; Katz, H. E. Marks, T. J. *Angew. Chem., Int. Ed.* **2003**, *42*, 3900. (j) Chesterfield, R. J.; Newman, C. R.; Pappenfus, T. M.; Ewbank, P. C.; Haukaas, M. H.; Mann, K. R.; Miller, L. L.; Frisbie, C. D. *Adv. Mater.* **2003**, *15*, 1278. (k) Babel, A.; Janekhe, S. A. *J. Am. Chem. Soc.* **2003**, *125*, 13656. (l) Shim, M.; Javey, A.; Kam, N. W. S.; Dai, H. *J. Am. Chem. Soc.* **2001**, *123*, 11512. (m) Dodabalapur, A.; Lin, Y. Y.; Filas, R. W.; Bao, Z.; LaDuca, A.; Sarpeshkar, R.; Katz, H. E.; Li, W. *Nature* **2000**, *403*, 521.

(10) Facchetti, A.; Yoon, M.-H.; Stern, C. L.; Katz, H. E.; Marks, T. J. *Angew. Chem., Int. Ed.* **2003**, *42*, 3900.

Experimental Section

Materials. The new oligothiophenes **2**, **3**, and **7**−**9** were prepared in 60−80% yields by $Pd[PPh_3]_4$-catalyzed Suzuki and/or Stille coupling reactions,[11] purified by gradient vacuum sublimation, and characterized by elemental analysis, mass spectrometry, and NMR spectroscopy. Synthetic details are reported in the Supporting Information. **1** and fluoroarene−thiophenes **4**−**6** were synthesized according to literature procedures (see Supporting Information).

5,5′-Bis{1-[4-(thien-2-yl)phenyl]}-2,2′-dithiophene (2). mp 370 °C. Anal. Calcd for $C_{28}H_{18}S_4$: C, 69.67; H, 3.76; Found: C, 69.65; H, 3.63. ^{1}H NMR ($C_2D_2Cl_4$, 100 °C): δ 7.67 (8H), 7.40 (2H), 7.47−7.30 (4H), 7.25 (2H), 7.15 (2H).

4,4′-Bis[5-(2,2′-dithiophenyl)]-biphenyl (3). mp 322 °C. Anal. Calcd for $C_{28}H_{18}S_4$: C, 69.67; H, 3.76; Found: C, 69.64; H, 3.75. ^{1}H NMR ($C_2D_2Cl_4$, 100 °C): δ 7.72 (10H), 7.32 (2H), 7.28 (2H), 7.23 (2H), 7.10 (2H).

5,5″-Diperfluorophenyl-2,2′:5′,2″-terthiophene (7). mp 186 °C. Anal. Calcd for $C_{24}H_6F_{10}S_3$: C, 49.66; H, 1.04; F, 32.73. Found: C, 49.43; H, 1.02; F, 33.14. ^{1}H NMR ($C_2D_2Cl_4$): δ 7.50 (d, 2H, ^3J = 3.5 Hz), 7.29 (d, 2H, ^3J = 3.5 Hz), 7.23 (s, 2H); ^{19}F NMR ($C_2D_2Cl_4$): δ −138.29 (4F), −154.10 (2F), −160.35 (4F).

5,5′-Diperfluorophenyl-2,2′-dithiophene (8). mp 183 °C. Anal. Calcd for $C_{20}H_4F_{10}S_2$: C, 48.20; H, 0.81; F, 38.12. Found: C, 47.92; H, 0.79; F, 38.48. ^{1}H NMR ($C_2D_2Cl_4$): δ 7.51 (d, 2H, ^3J = 3.5 Hz), 7.35 (d, 2H, ^3J = 3.5 Hz), 7.23 (s, 2H); ^{19}F NMR ($C_2D_2Cl_4$): δ −138.18 (4F), −153.86 (2F), −160.27 (4F).

5,5-Diperfluorophenylthiophene (9). mp 109 °C. Anal. Calcd for $C_{16}H_2F_{10}S$: C, 46.17; H, 0.48; F, 45.54. Found: C, 44.24; H, 0.59; F, 43.59. ^{1}H NMR ($C_2D_2Cl_4$): δ 7.62 (s, 2H); ^{19}F NMR ($C_2D_2Cl_4$): δ −137.86 (4F), −152.94 (2F), −160.01 (4F).

Thin Film Growth and Device Fabrication. All OTFT devices were fabricated by evaporating **1**−**9** (growth rate = 0.2−0.4 Å s^{-1}, $P \approx 10^{-6}$ Torr, film thickness = 50 nm) onto hexamethyldisilazane-treated p^+-Si/SiO_2 (300 nm oxide) substrates (or glass substrates for film optical measurements) maintained at 60 °C, and were completed by evaporating Au source and drain electrodes (50 nm thickness) through a shadow mask. Mobilities (μ) were calculated in the saturation regime from the relationship: $\mu_{sat} = (2I_{DS}L)/[WC_{ox}(V_G - V_{th})^2]$, where I_{DS} is the source-drain saturation current, W (5 mm) and L (100 μm) are the channel width and length, respectively, C_{ox} (10 nF/cm^2) is the gate oxide capacitance, V_G is the gate voltage, and V_{th} is the threshold voltage. For additional thin-film and device characterization information, see Supporting Information.

Results and Discussion

In the following, we discuss the molecular structures and electronic energetics of semiconductors **1**−**9** as defined by single-crystal X-ray diffraction (XRD), thermal analysis, optical and photoluminescence spectroscopy, and electrochemistry, as well as their thin-film microstructures and morphologies as characterized by XRD and scanning electron microscopy (SEM). Finally, this is followed by characterization of semiconductors **1**−**8** in OTFT devices.

Crystal Structures. Although phenylene−thiophenes with varying shapes and molecular connectivities have been synthesized and investigated, there are relatively few reports on the crystal structures of this type of molecule.[12] Examples of previously reported crystal structures include α,ω-bis[biphenyl-yl]-*n*Ts and two phenylene−thiophene oligomers. Crystals of the new oligomers **3** and **7**−**9** were grown by either slow vacuum sublimation or by slow cooling of saturated solutions. Crystallographic details are reported in Table S1.[13] Comparison between the crystal structures of these compounds with those of fluoroarene−thiophenes **4**−**6** provides insight into how arene fluorination and thiophene core length affect molecular structure and packing characteristics. The crystal structures of fluoroarene−thiophenes **7**−**9** exhibit the common feature of close cofacial organization of either the entire molecule or molecular fragments (vide infra) to bring the electron-rich (thiophene) and electron-deficient (perfluoroarene) subunits (Figure 1) into close proximity, as previously observed for mixed fluoroarene−thiophenes **4**−**6**[10] and other similar structures reported elsewhere.[14] In contrast, unsubstituted and alkyl/perfluoroalkyl-substituted oligothiophenes and phenylene−thiophene co-oligomers exhibit typical herringbone packing motifs.[12,15]

The molecular structures of the longer perfluoroarene end-substituted oligomers **4** and **7** (Figure 1) reveal substantially planar cores with a maximum core torsion of ∼17° (between the innermost two thiophene rings) and 8° (between the perfluorophenyl and outer thiophene rings), respectively. Radically different are the molecular structures of the shorter oligomers **8** and **9**, where one of the perfluorophenylene groups is twisted with respect to the remainder of the essentially planar molecule by angles of ∼36 and ∼22°, respectively. These angles are substantially greater than in typical unsubstituted oligothiophenes (∼5°)[15] and approach or exceed the ∼30° maximum value beyond which there is insufficient intramolecular π overlap to support a significant conduction band structure.[16] Whereas molecules of **4** exhibit an unusual syn conformational relationship between outer pairs of thiophene rings, the end-substituted systems **7** and **8** display typical all-trans conformations of the thiophene cores. The nonmonotonic contraction of the molecular length from **4** to **7**−**9** [24.21 Å (**4**), 21.33 Å (**7**), 17.46 Å (**8**), 13.49 Å (**9**)] reflects the differing distances between 1,4-fluoroarene (∼2.8−2.9 Å) and 2,5-thiophene (∼2.5 Å) ipso carbon atoms as well as the aforementioned different molecular conformations. Molecular packing is also quite different in the contrasting cases of the longer and shorter oligomers. The large core dimension of molecule **4** (as in the case of molecules **5** and **6**) allows each perfluorophenyl ring to interact intermolecularly with two of the four core thiophenes of a neighboring molecule, resulting in interleaved parallel layer stacking along the *b* axis with displacement of each molecular layer by one-half a molecule with respect to the neighboring layer. The minimum interlayer distances between cofacial molecules in adjacent planes is 3.20 Å (F_4−C_6'), comparable to or smaller than the sum of F−C (3.15−3.30 Å), S−C (3.45−3.50 Å), and C−C (3.30−3.40 Å) van der Waals radii.[17] In contrast, for the shorter oligothiophenes **8** and **9**, only one of the two perfluorophenyl rings can engage in face-to-face stacking with a

(11) March, J. In *Advanced Organic Chemistry: Reactions, Mechanisms, and Structure*; Wiley: New York, 1992.
(12) (a) Hotta, S.; Goto, M.; Azumi, R.; Inoue, M.; Ichikawa, M.; Taniguchi, Y. *Chem. Mater.* **2004**, *16*, 237. (b) Nagawa, M.; Hibino, R.; Hotta, S.; Yanagi, H.; Ichikawa, M.; Koyama, T.; Taniguchi, Y. *Appl. Phys. Lett.* **2002**, *80*, 544.
(13) All measurements were made on a CCD area detector instrument with graphite-monochromated Mo Kα (0.71073 Å) radiation. The data were collected at 153(2) K, and the structures were solved by direct methods and expanded using Fourier techniques. See Supporting Information for crystallographic details.
(14) . (a) Cho, D. M.; Parkin, S. R.; Watson, M. D. *Org. Lett.* **2005**, *7*, 1067. (b) Crouch, D. J.; Skabara, P. J.; Heeney, M.; McCulloch, I.; Coles, S. J.; Hursthouse, M. B. *Chem. Commun.* **2005**, 1465. (c) Reichenbaecher, K.; Heike, S. I.; Juerg. H. *Chem. Soc. Rev.* **2005**, *34*, 22.
(15) Fichou, D. *J. Mater. Chem.* **2000**, *10*, 571.
(16) (a) McCullough, R. D. *Adv. Mater.* **1998**, *10*, 93. (b) Brédas, J.-L. *J. Chem. Phys.* **1985**, *82*, 3809.
(17) Huheey, J. E.; Keiter, E. A.; Keiter, R. L. *Inorganic Chemistry*; Harper Collins College Publishers: New York, 1993; p. 292.

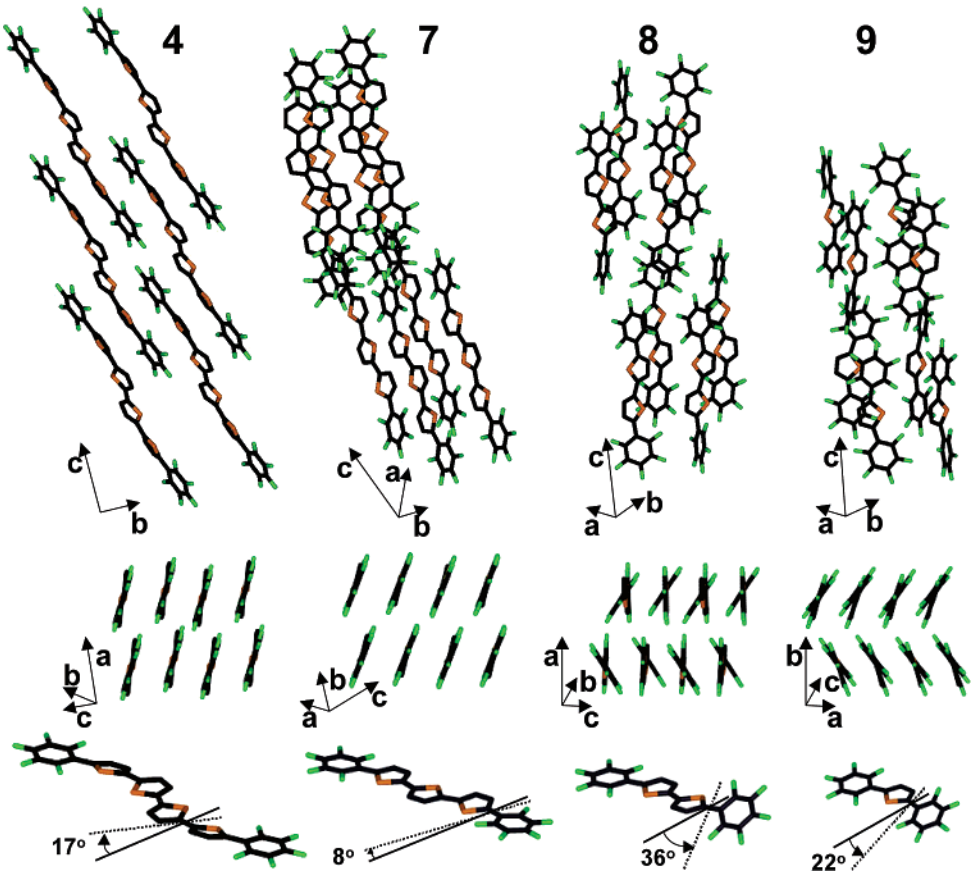

Figure 1. Crystal structures of semiconductors **4** and **7**−**9** showing packing characteristics and interring torsional angles.

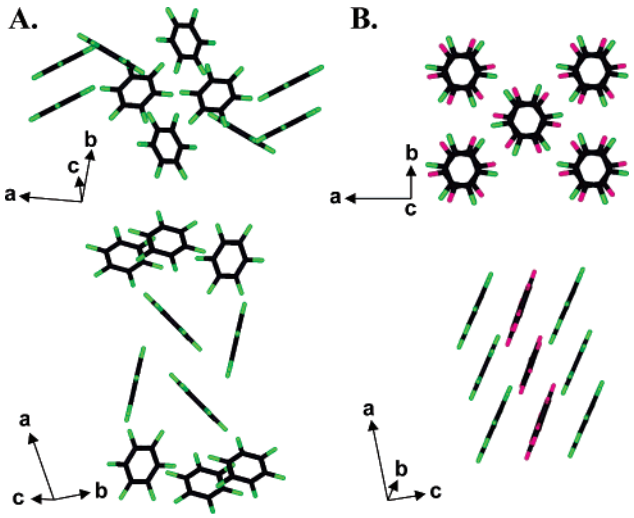

Figure 2. Crystal structure packing diagrams of A. perfluorobenzene, B. perfluorbenzene-C_6D_6 from the Cambridge Crystallographic Database.

neighboring electron-rich thiophene molecular fragment, with the consequence that the packing of part of the molecule is $\pi-\pi$ cofacial and the remaining perfluorophenyl unit packing is herringbone-like, with π-edge interactions, as found in the crystal structure of perfluorobenzene (see Figure 2).[18]

A more complex packing is observed for molecule **7**. In this case, the core planarity yields molecular layers extending along the *ab* plane in which the molecules within the layer are face-to-face stacked, whereas those of alternating layers intermingle, with their end perfluoroarene groups arranged in a herringbone fashion. The minimum intermolecular distances between cofacial molecular fragments/molecules are 3.49 Å (C_2-S_1') for **9**, 3.72 Å ($C_{17}-S_1'$) for **8**, and 3.32 Å (F_2-S_3') for **7**. These values are much greater than that observed in **4** (3.20 Å), probably because of the reduced number of closely $\pi-\pi$ stacked rings.

Figure 3 compares the crystal structures of the arene− and fluoroarene−thiophene oligomers **3** and **6**. The effect of arene fluorination is particularly evident in the change of molecular structure and packing. In contrast to that of **3**, the solid-state structure of **6** exhibits a very large intramolecular torsional angle (53.9°—slightly smaller than in typical perfluorobiphenyls)[19] between adjacent fluoroarene rings, hence interrupted π-conjugation. This is the result of the larger van der Waals radius (and greater electron density) of fluorine (1.47 Å) compared to that of hydrogen (1.20 Å).[17] Although **3** is structurally "wavey", the maximum dihedral angles between adjacent rings is only ∼5.7°, resulting in a substantially conjugated core. Due to the lack of electron-deficient rings, phenylene−thiophene **3** packs in the conventional herringbone motif with molecular stacking in the *ab* plane at a minimal intermolecular distance of 3.77 Å ($C_{11}-C_{13}'$). The herringbone canting angle is ∼50°, inbetween those reported for other phenylene−thiophene oligomers (48−70°).[12] In contrast, the packing of **6** is more complex, with waved layers having the long molecular axes extending along *a* (Figure 3) and slipping one-half with respect to the nearest neighbor molecule. In each layer, **3** molecules adopt a slipped cofacial stacking motif along *b* with sizable contacts between coplanar molecular subunits. The minimum interplanar distance

(18) Bertolucci, M. D.; Marsh, R. E. *J. Appl. Cryst.* **1974**, *7*, 87.

(19) Gleason, W. B.; Britton, D. *Cryst. Struct. Comm.* **1976**, *5*, 483.

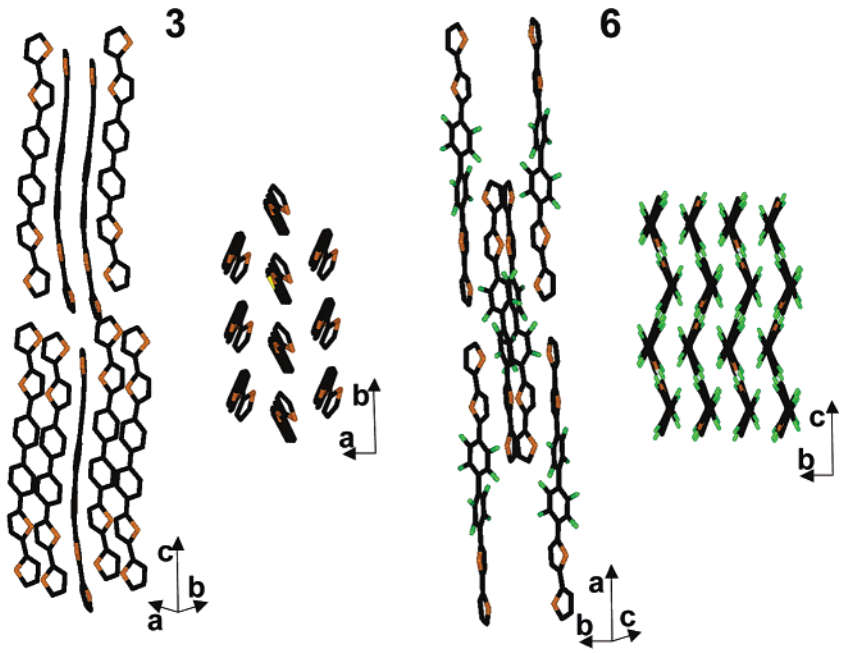

Figure 3. Crystal structure packing diagrams of semiconductors **3** and **6**.

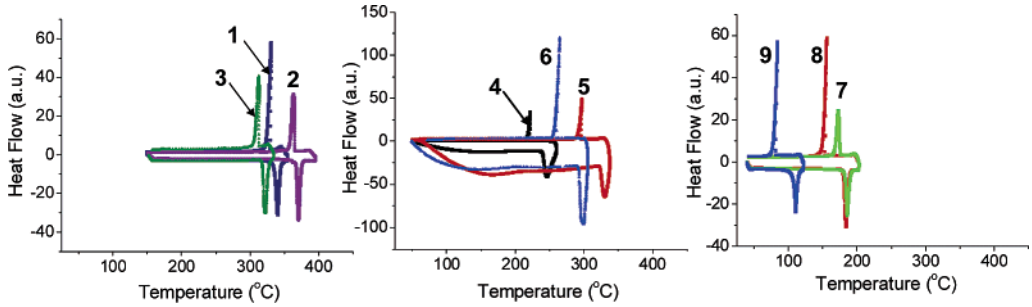

Figure 4. Differential scanning calorimetry (DSC) thermogram of compounds **1**−**9** (under N_2). The temperature ramp was 5-10 °C/min, and data were collected in the second scan cycle.

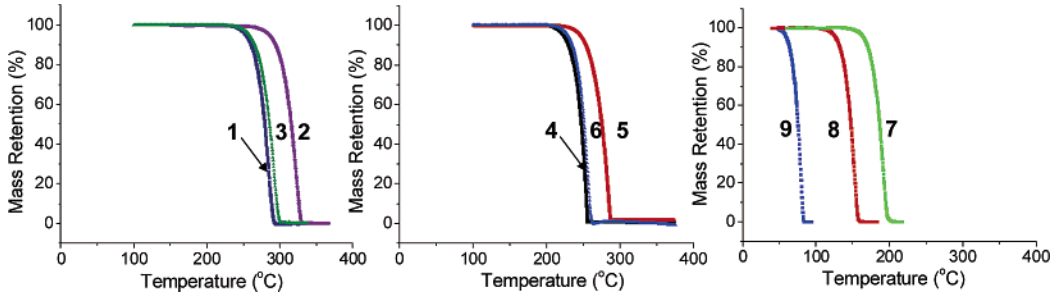

Figure 5. Volatility characteristics of semiconductors **1**−**9** by thermogravimetric analysis (TGA) at reduced pressure (0.1 Torr). The temperature ramp was 1.5 °C/min.

is 3.36 Å (S_1−F_3'). In contrast, close cofacial π−π stacking along *b* is unfavorable because rings of the same type would overlap. To accommodate this repulsion, a herringbone motif is formed with a minimum interstack distance of 2.88 Å (F_2−F_3) and a 59.9° canting angle.

Molecular Characterization. Differential scanning calorimetry (DSC) was performed for all the new fluoroarene−oligothiophenes and reveals (Figure 4) that the entire set of new compounds are thermally stable, with the DSC plots showing no evidence of mesophase formation before melting. This is surprising considering the rodlike structure of these systems and the observation of LC transitions for other phenylene−thiophene co-oligomers.[20]

Thermogravimetric analysis (TGA) of the present oligomers reveals quantitative sublimation in all cases (Figure 5), demonstrating volatility and the thermal robustness of these cores. Note that in contrast to the alkyl-substituted and the longer unsubstituted oligothiophenes[8b] and despite the very high melting points (Table 1), the nonfluorinated oligomers **1**−**3** also undergo sublimation without significant decomposition. Therefore, phenylene−thiophene ring admixing enhances thermal

(20) Dingemans, T. J.; Murthy, S. N.; Samulski, E. T. *J. Phys. Chem. B* **2001**, *105*, 8845.

Table 1. Melting Point, Optical Absorption Maxima (λ_{abs}), Fluorescence Emission Maxima (λ_{em}), and Electrochemical Potentials[a] for Compounds **1**−**9**

		λ_{abs} (nm)		λ_f (nm)		E_{gap} (eV)		E_{ox} (V)		E_{red} (V)	
compd.	mp(°C)	THF	film[b]	THF	film[b]	THF	film	$E_1^{1/2}$	$E_2^{1/2}$	$E_1^{1/2}$	$E_2^{1/2}$
1		423	358, 406, 503	494, 526	573, 618	2.61	2.47	+1.02	+1.20	−1.74	−1.94
2	370	399	345, 472	463, 494	540, 582	2.77	2.64			−1.77	−1.99
3	322	376	347, 418, 448	432, 456	500, 528	2.96	2.77	+1.23[c]	+1.43[c]	−1.63	
4	246	415	359, 442, 485	509, 540	437, 561	2.63	2.58	+1.19	+1.48	−1.51	−1.65
5	319	389	359, 420, 458	496, 525	547	2.82	2.65	+1.60[c]	+1.85[c]	−1.54	−1.66
6	285	371	364, 399, 434	459, 486	475	3.00	2.90	+1.58[c]		−1.55	−1.86
7	186	395	374, 426, 465	464, 490	535	2.98	2.65	+1.37	+1.49	−1.58	−1.70
8	183	357	365, 305, 416	423, 438	504	3.05	2.98	−1.71[c]		−1.62	−1.85
9	109	303		354, 367		3.36		+2.10[c]		−1.68	−2.04

[a] Referenced to the Fc^+/Fc couple in 0.1 mM tetrabutylammonium hexafluorophosphate/THF (0.54 V vs. SCE). Cyclic voltammetry measurements were performed at −10 °C with a C disk working electrode, a bare Ag reference electrode, and a Pt wire counter electrode. [b] 50 nm thick film vacuum deposited on glass. All spectra taken at room temperature. [c] Irreversible oxidation.

stability versus simple oligothiophenes. Furthermore, comparison of the TGA plots of **1**−**3** with those of **4**−**6** confirms that arene fluorination significantly enhances volatility, although the effect is not as dramatic as that observed on going from the alkyl- to fluoroalkyl-substituted oligothiophenes.[8b,8i,10] The volatility also increases when the thiophene core dimension is reduced, going from **4** to **7**−**9**. Indeed, films of the shorter oligomers **7** and **8** can be fabricated via vapor-deposition under relatively modest vacuum (ca 10^{-2} Torr), and **9** is so volatile that the corresponding films cannot be grown using standard semiconductor vacuum deposition apparatus.

Optical absorption and fluorescence emission spectra of **1**−**9** were measured both in solution and as thin films (with the exception of **9**) to assess the effect of arene location [**1**/**4** ↔ **2**/**5** ↔ **3**/**6**], fluorophenyl- vs pheny-substitutions [(**1**−**3**) ↔ (**4**−**6**)], and oligothiophene core shortening [**4** → **7** → **8** → **9**] on the molecular absorption/emission maxima ($\lambda_{abs}/\lambda_{em}$) and the HOMO−LUMO (optical) energy gap (E_{gap}). Table 1 collects UV−vis/PL data for all compounds in THF solution and as 50 nm-thick films on glass substrates. The solution absorption spectra of **1**−**9** are devoid of fine structure, whereas splitting of bands due to vibronic coupling can be clearly seen in the fluorescence spectra at room temperature (Figure S1). This coupling is due to planarization of the system upon excitation. The solution ground state is on average more twisted than is the excited state, in agreement with the latter state having greater quinoid character. The periodicity in the splitting is ∼1400−1500 cm^{-1} and can therefore be attributed to one of the ν(C=C) stretching modes of the aromatic core.[21]

Compared to unsubstituted sexithiophene (α**6T**; λ_{abs} = 427 nm, λ_{em} = 371 nm),[10] it can be seen from Table 1 that both λ_{max} and λ_{em} in THF systematically fall in the order α**6T** > **1**/**4** > **2**/**5** > **3**/**6**. These trends indicate that replacement of thiophene by an arene ring [α**6T** → (**1**−**6**)] incurs substantial steric repulsions, resulting in pronounced distortion from planarity. Other possible effects on absorption positions such as differing sensitivities to solvent dielectric constant (solvatochromism) and/or aggregation can be excluded.[22] When comparing the absorption of the phenylene−thiophene and fluoroarene−thiophene systems having the same core architecture, λ_{abs} values shift hypsochromically by ∼8 nm (**1** → **4**), ∼11 nm (**2** → **5**), and ∼5 nm (**3** → **6**), probably because of the greater steric demands of F versus H. However, such geometric effects on λ_{abs} are not as large as would have been predicted by comparing the crystal structures of **3** (well conjugated) and **6** (essentially deconjugated). This result suggests that the structures of **1**−**3** and **4**−**6** are more similar in solution, meaning that the former systems are probably less conjugated in solution. Additionally, it can be seen in Table 1 that λ_{abs} and λ_{em} are incrementally shifted to higher energy as the six-membered rings are displaced toward the molecular core [**1** → **2** → **3** and **4** → **5** → **6**], reflecting the greater steric demands of six- versus five-membered rings. Consequently, solution optical HOMO−LUMO energy gaps (eV) decrease from ∼3.0 (**3**/**6**) to ∼2.8 (**2**/**4**) to ∼2.6 (**1**/**3**) to 2.55 for α**6T**. As expected, when end-substituted fluoroarene−oligothiophenes are considered, solution λ_{abs} values decrease for decreasing numbers of thiophene core units. The trend in this shift [$\Delta\lambda_{abs}$ (nm) = 20 (**4** → **7**), 38 (**7** → **8**), 54 (**8** → **9**)] is similar to that observed for other oligothiophene classes in the same solvent.[8b] However, the present λ_{abs} values are substantially blue-shifted compared to the corresponding unsubstituted α*n*T oligothiophenes having the same number of π-electrons [e.g., $\Delta\lambda$ = 54 nm (**9** → α**3T**) and 23 nm (**7** → α**5T**)] with the displacement in maximum absorption ($\Delta\lambda$) increasing as the number of rings is decreased. This result is in accord with the greater fluoroarene steric demands.

UV−vis/PL data for vacuum-deposited thin films of **1**−**8** are also summarized in Table 1. The absorption spectra (Figure S2) exhibit characteristic peak(s) at high energy (270−280 nm, not shown) found in the optical spectra of all oligothiophenes and centered in the thiophene (and arene) ring.[23] The position and shape of the $\pi \rightarrow \pi^*$ transition(s) reflects the interplay of molecular structure, substitution, core length, and solid-state packing. Compared to the solution spectroscopic data, thin-film measurements indicate different trends for both λ_{max} and λ_{em}, which exhibit hypsochromic and bathochromic shifts, respectively, for **1**−**5**, **7**, and **8**, whereas the data for **6** shift oppositely. These results suggest different coupling between molecular transition dipoles (H- and J-type aggregates, respectively), and allow within a Frenkel exciton model[24] estimation of film E_{gap}

(21) (a) Garnier, F. *Acc. Chem. Res.* **1999**, *32*, 209. (b) Yassar, A.; Horowitz, G.; Valat, P.; Wintgens, V.; Hmyene, M.; Deloffre, F.; Srivastava, P.; Lang, P.; Garnier, F. *J. Phys. Chem.* **1995**, *99*, 9155.

(22) The λ_{abs} and λ_{em} values for α**6T** and **1**−**6** change little on going from polar THF to less polar toluene and for experimental concentrations < 10^{-5} M.

(23) Yassar, A.; Horowitz, G.; Valat, P.; Wintgens, V.; Hmyene, M.; Deloffre, F.; Srivastava, P.; Lang, P.; Garnier, F. *J. Phys. Chem.* **1995**, *99*, 9155.

(24) (a) Klessinger, M.; Michl, J. *Excited States and Photochemistry of Organic Molecules*; VCH Publisher: New York, 1995. (b) Pope, M.; Swenberg, C. E. In *Electronic Processes in Organic Crystals and Polymers*; Oxford University Press: Oxford, 1999.

values using the longest λ absorption maxima, which appear as forbidden, low-intensity features in the former systems, and as an allowed, high-intensity excitation for **6** (Davidov splitting). A film E_{gap} (eV) ordering ~2.8−2.9 (**3**/**6**) > ~2.65 (**2**/**4**) > ~2.5−2.6 (**1**/**3**) > 2.42 for α**6T 3** is thereby estimated and leads to two interesting conclusions. First, monotonic $\lambda_{max}/\lambda_{em}$ shifts and band shape differences between **6** and the other compounds/films are consistent with the very different solid-state packing. Second, the larger **2**/**4** film E_{gap} diminution (~0.2 eV), approaching the values for **1**/**4** and α**6T**, is consistent with some planarization of the structure of **4** (as seen in the diffraction results above) and probably that of **2** on going from solution to the condensed state. The average greater conjugation in the solid state is confirmed by comparing the optical gaps in solution and in thin films, with the latter being about 0.2−0.5 eV smaller.

The electrochemical properties of oligo and polythiophenes have been extensively investigated and reveal important chemical and electronic structure-materials performance trends.[25,26] However, to the best of our knowledge, electrochemical data for phenylene−thiophene co-oligomers have not been reported. Cyclic voltammetry (CV) studies of oligomers **1**−**9** were performed under N_2 in 0.1 M THF/$TBAPF_6$ solutions with scan rates between 80 and 100 mV/s. With the exception of **3**, all systems exhibit two reversible and/or quasi-reversible one-electron reduction waves within the span of the solvent/electrolyte window. Figure S3 shows representative voltammograms. In cases where the voltammograms are (quasi)reversible, it is possible to extract formal potentials ($E^{1/2}$) as the midpoints between the peak potentials of the forward and reverse scans, and the data are summarized in Table 1. In contrast to a number of oligothiophene families,[8,10] there appears to be no relationship in the present case between the chemical stability of **1**−**9** as oxidized or reduced species and the extension of the core or variation of the substitution. This can be judged from the fact that both $E^{1/2}{}_1$ and $E^{1/2}{}_2$ reductions can be observed for almost all systems investigated, whereas reversible $E^{1/2}{}_1$ and $E^{1/2}{}_2$ processes are observed for a larger arene−thiophene core (**1**), a larger fluoroarene−thiophene core (**5**), and a smaller fluoroarene−thiophene core (**7**). Analysis of the half-wave potentials reveals the importance of arene fluorination in modulating MO energetics.

Compared to phenylene−thiophenes **1**−**3**, the reduction (and oxidation for **1**) potentials $E^{1/2}{}_1$ and $E^{1/2}{}_2$ of the corresponding fluoroarene systems **4**−**6** (and oxidation for **4**) are shifted toward larger values by ~0.2 V, in agreement with the electron-withdrawing capacities of fluoroarene vs arene rings. As a function of molecular core length compression [**4** → **7** → **8** → **9**], the $E^{1/2}{}_1$ and $E^{1/2}{}_2$ reduction parameters (and oxidations for **4** and **7**) are displaced to more negative (more positive) values. This trend indicates a progressive increase of the (electrochemical) band gap, in excellent agreement with the aforementioned optical data. Furthermore, the potential difference between subsequent reduction events [$\Delta E^{1/2} = |E^{1/2}{}_2 - E^{1/2}{}_1|$] increases as the core length decreases [e.g., $\Delta E^{1/2} = 0.14$ V for **4** and 0.36 for **9**], consistent with increased Coulombic repulsion between excess delivered charge. A similar trend was observed for the α*n*T and phenylene (*p*-*n*P) series.[8,27]

Table 2. *d*-Spacings (Å), Majority Charge Carrier Type, Field-Effect Mobilities (μ, cm^2/Vs) and Current $I_{on}:I_{off}$ Ratios as a Function of Growth Temperature (T_D, °C) for Vapor-Deposited Films of the Indicated Semiconductors (50 nm) on HMDS-treated Si/SiO_2 Substrates[a]

			Deposition Temperature (T_D)					
			25 °C		60 °C		90 °C	
semiconductor	*d*-spacing	type	μ	$I_{on}:I_{off}$	μ	$I_{on}:I_{off}$	μ	$I_{on}:I_{off}$
1	23.9	P	0.02	10^5	0.07[b]	$>10^5$	0.09	10^6
2	24.9	P	0.03	10^6	0.03	10^6	0.04	$>10^6$
3	25.2	P	0.03	10^5	0.03	10^5	0.02	10^6
4[c]	25.1	N	0.01	10^3	0.07	$>10^6$	0.43	$>10^8$
5	18.4/15.0	P	0.005	10^4	0.01	$>10^5$	0.004	$>10^5$
6	6.0	P	0.00002	10	0.00004	10^4	NA[d]	NA[d]
7	14.0	N	0.0002	10^2	0.002	10^5	0.003	$>10^4$
8	18.8	N	<0.00001	10	0.00001	10^2	0.00001	10^2

[a] SiO_2 dielectric (300 nm, $C_i = 10$ nF/cm^2); $L = 100$ μm, $W = 5$ mm. Measured in a Ar-refilled probe station. [b] $\mu = 0.033$ cm^2/Vs from ref [6d]. [c] At $T_D = 110$ °C $\mu = 0.22$ cm^2/Vs $I_{on}:I_{off} = 10^7$. [d] NA: Not active.

Thin-Film Morphology. Film microstructure and morphology for this new class of materials were studied by XRD and SEM for 50 nm films vacuum-deposited at 60 °C on HMDS-treated Si/SiO_2 substrates. All films were grown under identical conditions of pressure and growth rate for accurate comparison. $\theta - 2\theta$ X-ray diffraction spectra of the new oligomer films reveal that all of the films are characterized by a high degree of texture, with *d*-spacings indicating that the majority of the molecules have an edge-on growth orientation (Table 2; see more below). The only exception is the poorly conjugated fluoroarene **6**. Note that films of phenylene−thiophenes **1**−**3** exhibit only a single dominant Bragg progression (Figure 6), with the *d*-spacings falling within a very narrow range (24−25 Å), irrespective of regiochemical modifications. For **3**, the derived *d* spacing (25.2 Å) is practically identical to the *c* axis length observed in the crystal structure (25.3 Å), meaning that molecules of **3** are oriented with their long molecular axes parallel to the substrate normal with a tilt angle (ϕ) ≈ 0°.

Because the computed molecular lengths of **1**−**3** are very similar (and exhibit very similar solid-state optical characteristics), this result indicates that the corresponding films have very similar microstructures with all of the molecular long axes at a near-zero angle vs the substrate normal. In the marked contrast, fluoroarene−thiophenes **4**−**6** behave differently, with the films of **4** and **5** exhibiting edge-on molecular orientations along the substrate normal but with a tilting of ~25° (**4**) and ~43° (**5**), whereas films of **6** have the majority of the molecules oriented parallel to the substrate surface ($\phi \approx 90°$). The tilt angle (θ) was calculated from the molecular length (*l*) in the single-crystal diffraction data and the film *d* spacing (*d*, see Figure S5) determined from the film XRD ($d = l \cos \theta$). It will be seen that these differences greatly affect film electrical performance. Films grown from end-substituted **7** and **8** at 60 °C are also characterized by a very high degree of texture (Figure S4). However, single sets of sharp Bragg reflections are observed for **7** and **8**, but only after the films are subjected to brief

(25) (a) Jagur-Grodzinski, J. *Polym. Adv. Technol.* **2002**, *13*, 615−625. (b) Cravino, A.; Sariciftci, N. S. *J. Mater. Chem.* **2002**, *12*, 1931. (c) Wolf, M. O. *Adv. Mater.* **2001**, *13*, 545. (d) Fabre, B.; Simonet, J. *Coord. Chem. Rev.* **1998**, *178*, 1211. (e) Roncali, J. *Chem. Rev.* **1992**, *92*, 711.

(26) (a) Domagala, W.; Laokowski, M.; Guillerez, S.; Bidan, G. *Electrochim. Acta* **2003**, *48*, 2379. (b) Briehn, C. A.; Schiedel, M.-S.; Bonsen, E. M.; Schuhmann, W.; Bauerle, P. *Angew. Chem., Int. Ed.* **2001**, *40*, 4680. (c) Nessakh, B.; Horowitz, G.; Garnier, F.; Deloffre, F.; Srivastava, P.; Yassar, A. *J. Electroanal. Chem.* **1995**, *399*, 97. (d) Meerholz, K.; Heinze, J. *Electrochim. Acta* **1996**, *41*, 1839.

(27) (a) Domagala, W.; Laokowski, M.; Guillerez, S.; Bidan, G. *Electrochim. Acta* **2003**, *48*, 2379. (b) Jagur-Grodzinski, J. *Polym. Adv. Technol.* **2002**, *13*, 615. (c) Meerholz, K.; Heinze, J. *Electrochim. Acta* **1996**, *41*, 1839.

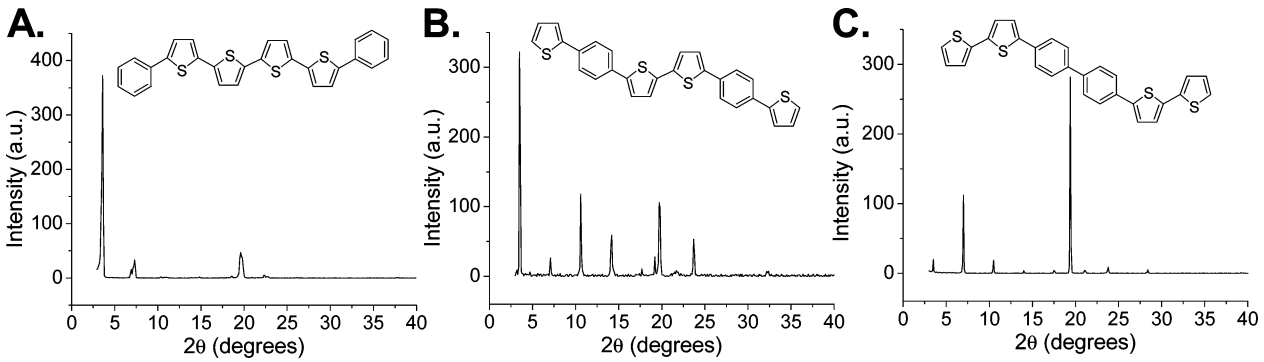

Figure 6. Film σ-2σ XRD data for 50 nm-thick films of the indicated semiconductors grown on HMDS-treated Si/SiO_2 substrates: A. **1**, B. **2**, and C. **3**.

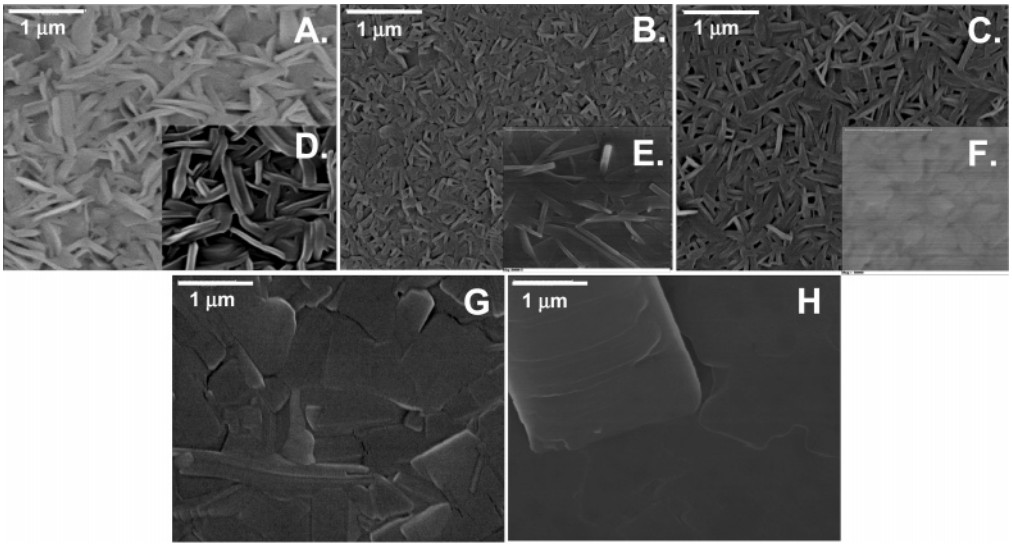

Figure 7. SEM images of 50 nm thick films of the following semiconductors grown on HMDS-treated Si/SiO_2 substrates at 60 °C: A. **1**, B. **2**, C. **3**, D. **4**, E. **5**, F. **6**, G. **7**, H. **8**. The Scale bar denotes 1 μm.

annealing ($T = 120$ °C for 40 min). The corresponding film d spacings are 14.0 Å for **7** and 18.8 Å for **8**, which correspond to one-half of the unit cell c axes, indicating molecular tilt angles of ~48 and ~0°, respectively. Consequently, in all cases except for **6**, the molecular orientation is favorable for efficient charge transport parallel to the SiO_2−semiconductor interface.

SEM images were recorded on films of semiconductors **1**−**8** (Figure 7), and differing morphological trends within each family are clearly visible. Films of **1**−**3** reveal highly interconnected μm-long rodlike crystallites and almost identical morphologies. However, morphologies in the perfluoroarene−thiophene series **4**−**6** are highly dependent on molecular regiochemistry, with films of **4** and **5** consisting of highly interconnected crystallites and those of **6** being smoother and having rounded crystallite features. SEM images of the films derived from smaller oligomers **7** and **8** reveal a completely different morphology with highly intermingled and larger squared-shaped grains.

Thin-Film Transistor Fabrication and Characterization Measurements. The structure of the typical top-contact thin-film transistor fabricated in this study is shown schematically in the inset of Figure 8A. The present field-effect devices operate in accumulation, meaning that the source-drain current is enhanced (on-state) by the application of a negative and positive source-gate voltage for p- and n-channel semiconductors, respectively.[1a] When the source-gate voltage is zero, the device source-drain current should be very low (off-state) to ensure efficient current switching (high current on-to-off ratio). The key materials-device metrics are the semiconductor charge carrier mobility (μ) and the current on/off ratio (I_{on}/I_{off}), which can be calculated in the so-called saturation regime ($V_{SG} > V_{SD}$) from eq 1

$$I_{DS} = \frac{W}{2L}\mu C_i[V_G - V_T]^2 \qquad (1)$$

where W/L is the channel width/length (here 5000 μm/100 μm), C_i is the gate dielectric capacitance per unit area (here 10 nF/cm^2), V_G is the source-gate voltage, and V_T is the threshold voltage. Our devices consist of a p^+-Si gate-substrate, a 300 nm SiO_2 dielectric layer, a 50 nm-thick vapor-deposited **1**−**8** semiconductor film, and 50-nm thick top source-drain Au contacts. All measurements were performed in an Ar-filled probe station.Transistor activity is observed for all of the present semiconductor films but only when applying positive biases for **4**, **7**, and **8** (n-type) and negative biases for **1**−**3**, **5**, and **6** (p-type). Ambipolar behavior was not observed in any case. Table 2 summarizes majority carrier sign, mobilities, and I_{on}/I_{off} ratios for the present semiconductors at various substrate deposition temperatures (T_D). For p-type arene−thiophenes **1**−**3**, hole mobilities vary over a small range (0.02−0.09 cm^2/Vs) despite significant T_D changes and ring regiochemical arrangements, with I_{on}/I_{off} ratios of 10^5−10^6. Note that the optimized mobility

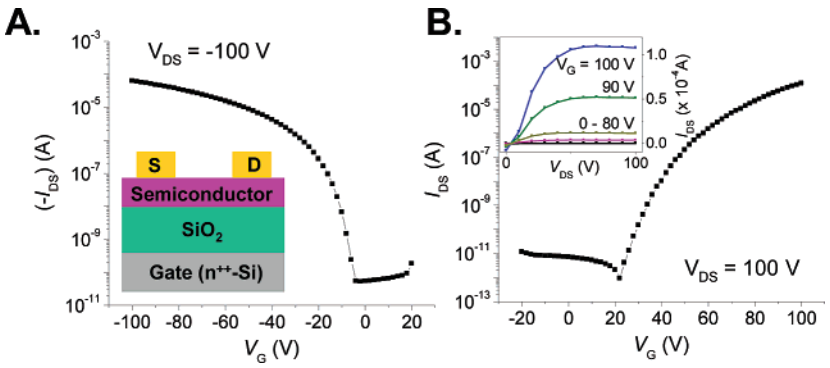

Figure 8. Transfer characteristics of TFT devices based on filsm of A. semiconductor **2** and B. semiconductor **4**. A inset: Schematic of a TFT device and B inset: Output plot of semiconductor **4** films.

values for **1**−**3** are very close to that reported for α**6T** (0.04−0.06 cm^2/Vs).[8b] In contrast, the corresponding I_{on}/I_{off} ratios are substantially greater (α**6T**; ∼10^4), confirming that the phenylene−thiophene cores are significantly more resistant to doping (vide infra).[6b,d] These results are also consistent with the more electron-deficient molecular structures as well as with the corresponding film microstructures and morphologies of these semiconductors. All of these films exhibit very similar molecular orientations and morphologies on the dielectric surface, whereas XRD, electronic structure computation,[28] and film UV−vis data suggest comparable π-conjugation and great similarity to mostly planar α**6T**.

In contrast to the phenyl−thiophene results, two important differences are observed for the perfluoroarene−thiophene series **4**−**6**. First, **5** and **6** are p-type semiconductors, whereas **4** is n-type, rendering this family the first regiochemically induced organic n-type material.[10] Second, within the fluoroarene−thiophene series, the mobilities (0.00001−0.5 cm^2/Vs) and the I_{on}/I_{off} current ratios (10^1−10^8) vary dramatically with molecular regiochemistry as well as with the substrate growth temperature. The change in majority carrier type from **1**−**3** to **4** most likely reflects the combined result of the LUMO energy-lowering arene perfluorination (∼0.2 eV effect in the electrochemical data) and possible fluoroarene core screening of residual O_2 at the grain boundaries, as suggested for other n-type organic semiconductors.[8,9] The regiochemically promoted majority carrier charge inversion from **4** to **5** and **6** is less obvious to rationalize, and a band structure analysis is currently in progress.[28]

In contrast to the above majority carrier issues, absolute variations in mobility and I_{on}/I_{off} ratio within the **4**−**6** series are readily explicable. The relatively large mobilities of **4**- and **5**-derived films compared to those of **6** are doubtless associated with the substantial core planarity of the former molecules as evident in the crystal structures, and the favorable film microstructures (vide supra). The greater scatter in μ values with T_D for **4**−**6** versus **1**−**3** is a typical feature of most fluorinated semiconductors developed in this laboratory[8,10] and reflects the greater sensitivity of the fluorinated semiconductor film microstructure/morphology to the film growth conditions (principally deposition temperature but also growth rate and substrate surface pretreatment). Interestingly, within the fluorinated series, note that this sensitivity is far greater for the n- versus the p-type systems; the mobility of **5** and **6** varies at most ∼3×, whereas that of **4** varies by more than ∼14×, confirming more facile electron trapping versus hole trapping by semiconductor impurities and film defects/grain boundaries at the dielectric-semiconductor interface. In particular, optimizing the growth conditions for films of **4** increases the TFT mobility to >0.4 cm^2/Vs with an exceptionally high $I_{on}/I_{off} > 10^8$. With the exception of pentacene, such very large values are unprecedented in polycrystalline films of *unsubstituted* (hetero)aromatic semiconducting oligomers (e.g., oligothiophenes, phenylenes, fluorenes, and co-oligomers), where performance is generally enhanced by alkyl-sustitution which enhances molecular packing and film crystallinity.[29] In the case of semiconductor **4**, the electron-rich/electron-deficient intermolecular interactions are sufficient to promote optimum molecular π−π overlap and excellent film texture. The shorter oligomers **7** and **8** are also n-type semiconductors, demonstrating that fluoroarene end-substitution promotes majority carrier sign inversion, independent of the thiophene core extension. However, the TFT figures of merit are greatly diminished compared to **4**, particularly for semiconductor **8**. Because the corresponding films exhibit a high degree of texture and optimum molecular orientation with respect source-drain charge transport directionality, the explanation may lie in the effective shorter π core. Indeed, the crystal structure of **8** reveals that only three rings are fully conjugated, making the electronic structure of this molecule closer to poor-mobility terthiophene than good-mobility quaterthiophene derivatives.[30]

Conclusions

The present study describes the realization and molecular/thin film properties of a new class of arene/fluoroarene−thiophene co-oligomers having sequential variation of arene−thiophene fragment positioning and thiophene core conjugation length. Trends in optical absorption and emission parameters, electrochemical potentials, film microstructure, and morphology can be directly correlated with thin-film electrical performance in field-effect devices. Field effect transistor measurements demonstrate that all of these systems are FET-active, with most oligomers exhibiting comparable p- or n-type mobility. Close π−π stacking in the unit cell and excellent film microstructure growth characteristics render **4** one of the highest mobility n-type

(28) Koh, S.; Facchetti, A.; Freeman, A. J.; Medevedeva, J.; Delley, L. D.; Ratner, M. A.; Marks, T. J. In preparation

(29) Dimitrakopoulos, C. D.; Malenfant, P. R. L. *Adv. Mater*. **2002**, *14*, 99.

(30) (a) Hutchison, G. R.; Ratner, M. A.; Marks, T. J. *J. Am. Chem. Soc.* **2005**, *127*, 16866. (b) Katz, H. E.; Torsi, L.; Dodabalapur, A. *Chem. Mater.* **1995**, *7*, 2235. (c) Garnier, F.; Hajlaoui, R.; El Kassmi, A.; Horowitz, G.; Laigre, L.; Porzio, W.; Armanini, M.; Provasoli, F. *Chem. Mater.* **1998**, *10*, 3334.

materials reported to date and provide new insights into the design of optimized molecular and polymeric organic semiconductors.

Acknowledgment. We thank ONR (N00014-02-0909), the NSF-MRSEC program through the Northwestern Materials Research Center (DMR-0076097), and the NASA Institute for Nanoelectronics and Computing (NCC 2-3163) for support.

Supporting Information Available: Synthesis of semiconductors **2**, **3**, and **7**−**9**, single crystallographic data, spectroscopic/electrochemistry data, XRD, and OTFT device fabrication. Figures S1−S5. This material is available free of charge via the Internet at http://pubs.acs.org. Crystal structures of semiconductors **4** and **7**−**9** showing packing characteristics and interring torsional angles. Crystal structure packing diagrams of (A) perfluorobenzene and (B) perfluorbenzene-C_6D_6 from the Cambridge Crystallographic Database. Crystal structure packing diagrams of semiconductors **3** and **6**.

JA060016A